Chapter 3

Attenuation Due to Roadside Trees: Mobile Case

3.1 Background

As of this writing, a limited number of LMSS related propagation investigations have been executed at UHF and L-Band where the transmitter platforms were located on satellites. A summary of other investigations is given in Chapter 7. LMSS propagation measurements with satellite transmitter platforms were conducted by the authors in central Maryland with MARECS-B2, [Vogel and Goldhirsh, 1990], and in Australia with the Japanese ETS-V and INMARSAT-Pacific satellites [Vogel et al., 1991; Hase et al., 1991]. Other types of transmitter platforms used for mobile measurements were also employed to derive propagation information for LMSS configurations. Vogel and Hong [1988] reported on stratospheric balloons carrying transmitters at 870 MHz and 1502 MHz where measurements were made in western Texas and New Mexico . Goldhirsh and Vogel [1989; 1987] and Vogel and Goldhirsh [1988] also describe helicopter experiments at both 870 MHz and 1.5 GHz in the central Maryland and north-central Colorado regions of the United States.

3.2 Time-Series Fade Measurements

In the analysis of times-series roadside fades for LMSS scenarios, the attenuation levels were represented by the dB ratio of the shadowed power received relative to the unshadowed levels under conditions of negligible multipath. Figures 3.1 and 3.2 are examples of measurements depicting nominal characteristics of time-series of fades (a) and phases (b) for non-shadowed and shadowed line-of-sight cases, respectively. These measurements were performed by Vogel et al. [1991] in Australia where L-Band transmissions (1.5 GHz) emanating from the Japanese ETS-V were received at an elevation angle of 50°. For the cases indicated in Figures 3.1 and 3.2, the vehicle speeds were approximately 17.4 m/s and 11 m/s for the unshadowed and shadowed cases, respectively. The receiver noise had fluctuations which were within 1 dB (rms). The unshadowed environment (Figure 3.1) may be characterized as a "flat rural region" and the shadowed case (Figure 3.2), a suburban location having roadside trees.

Fluctuations outside the one dB noise level in Figure 3.1 (a) are due to multipath. Nominally, peak-to-peak variations of less than 5 dB of power and 25° of phase were observed for non-shadowed cases. We note the shadowed case (Figure 3.2) has fades which are highly variable with fluctuations exceeding 15 dB. Some of these deep fades are also accompanied by rapid phase shifts.

Time-series of fade and phase of the above types were obtained for various LMSS geometries and environments and corresponding cumulative distributions were derived as described in the following paragraphs.

3.3 Empirical Roadside Shadowing Model

Cumulative L-Band fade distributions systematically derived from helicopter-mobile and satellite-mobile measurements in central Maryland enabled the formulation of an Empirical Roadside Shadowing (ERS) model. The measurements were obtained over approximately 600 km of driving distance comprising path elevation angles of 21°, 30°, 45°, and 60°. The 21° case was executed employing MARECS-B2 [Vogel and Goldhirsh, 1990], whereas the measurements for the other angles were obtained employing the helicopter as the transmitter platform. The configurations correspond to maximum shadowing conditions; namely, the

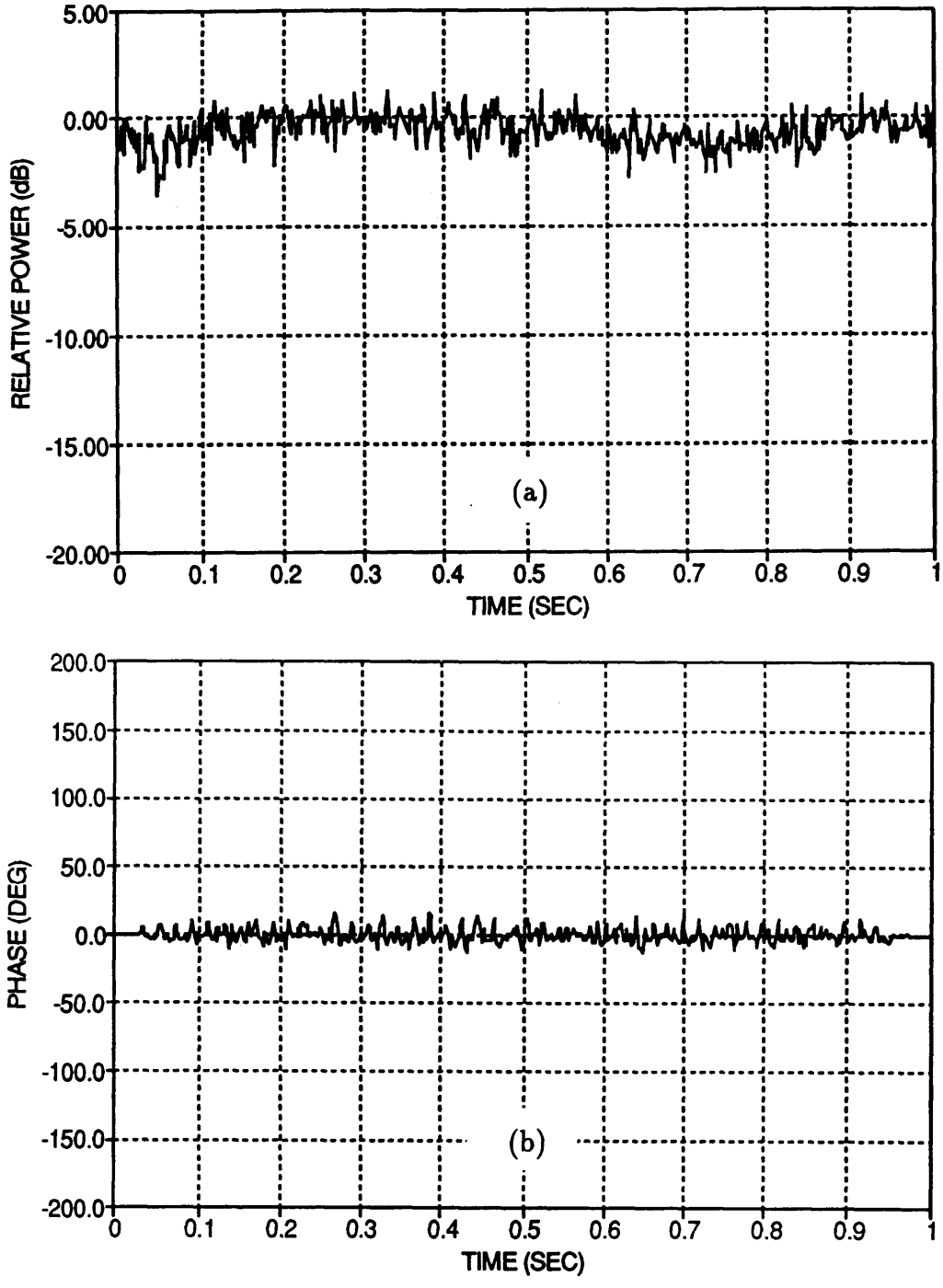

Figure 3.1: Time-series of fades (a) and phases (b) over a one second period at a sampling rate of 1 KHz in a flat rural region where the line-of-sight was unshadowed.

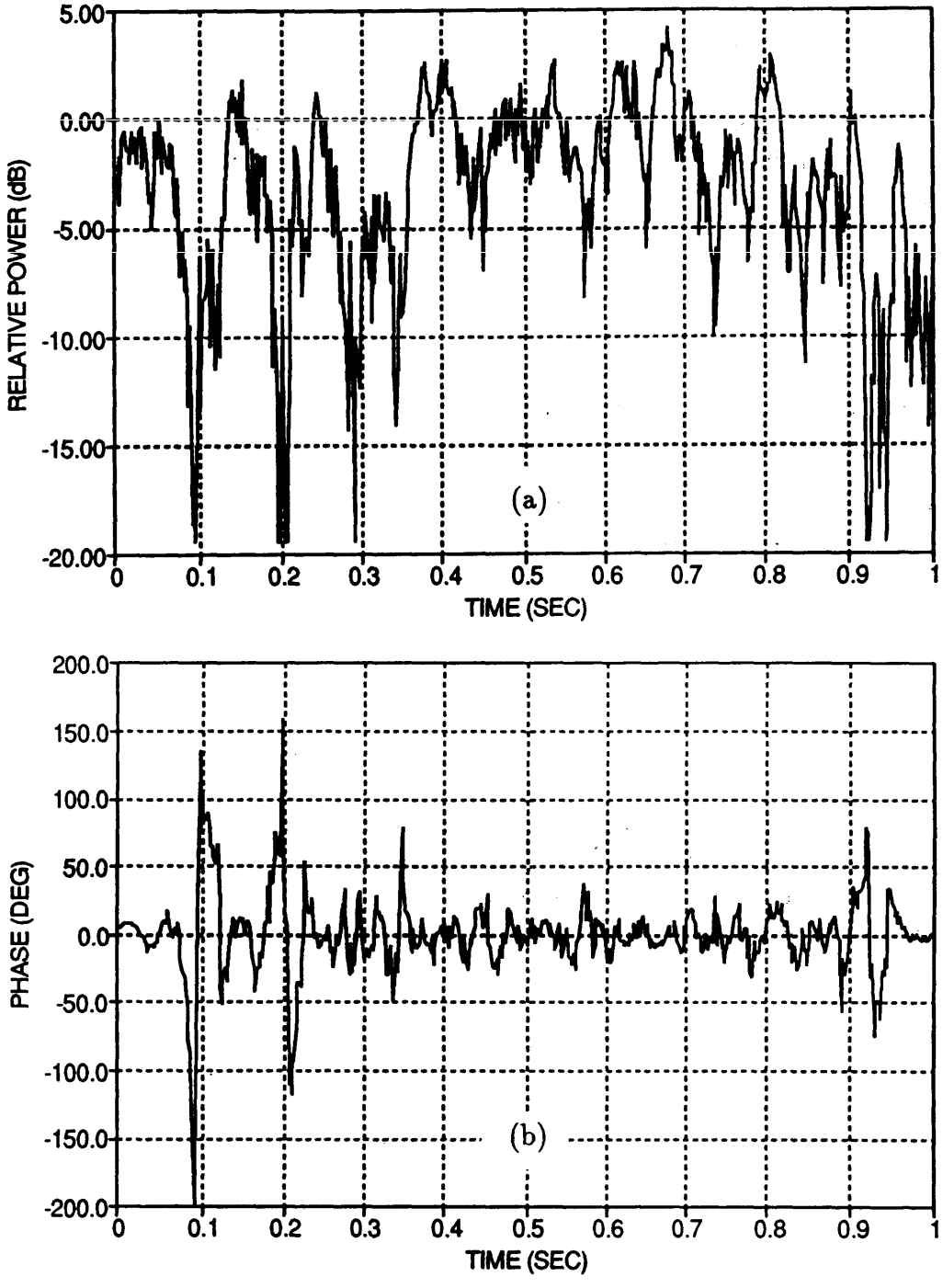

Figure 3.2: Time-series of fades (a) and phases (b) over a one second period at a sampling rate of 1 KHz in a suburban region with roadside trees where the line-of-sight was shadowed.

helicopter flew parallel to the moving vehicle and the propagation path was approximately normal to the line of roadside trees which ranged in height from approximately 5 to 30 m. The satellite path directions were such that they were also predominantly along the maximum shadowing orientation although some of the roads sampled have a number of bends in them and deviations from this aspect did arise. The measurements were performed on two lane highways (one lane each direction), and a four lane highway (two lanes each direction), where the roadside trees were primarily of the deciduous variety. In order to assess the extent by which trees populate the roadside, a quantity called percentage of optical shadowing (POS) was defined. This represents the percentage of optical shadowing caused by roadside trees at a path angle of 45° for right side of the road driving, where the path is to the right of the driver and the vehicle is in the right lane. The POS for the roads driven were predominantly between 55% and 75%.

The empirical expression, obtained by applying "best fit formulations" to the measured fade distributions at 1.5 GHz, is given by

<u>P = 1% to 20%</u>

$$A(P,\theta) = -M(\theta)\ln P + N(\theta) \tag{3.1}$$

where A is the fade in dB, P is the percentage of the distance traveled over which the fade is exceeded, and θ is the path elevation angle to the satellite. Since the speed was maintained nominally constant for each run, P may also be interpreted as the percentage of the time the fade exceeds the abscissa value.

Least square fits of second and first order polynomials in elevation angle θ (deg) generated for M and N, respectively, result in

$$M(\theta) = a + b\theta + c\theta^2 \tag{3.2}$$

$$N(\theta) = d\theta + e \tag{3.3}$$

where

$$\begin{cases} a = 3.44 \\ b = .0975 \\ c = -0.002 \\ d = -0.443 \\ e = 34.76 \end{cases} \tag{3.4}$$

Table 3.1: Coefficients M and N As a function of θ for Equation (3.1)

Path Angle θ (degrees)	M	N
20	4.590	25.90
25	4.628	23.69
30	4.565	21.47
35	4.403	19.26
40	4.140	17.04
45	3.778	14.83
50	3.315	12.61
55	2.753	10.40
60	2.090	8.18

The ERS model corresponds to an overall average driving condition encompassing right and left lane driving and opposite directions of travel along highways and rural roads where, as mentioned, the overall aspect of the propagation path was for the most part orthogonal to the lines of roadside trees and utility poles . The dominant causes of LMSS signal attenuation are due to canopy shadowing, where multipath fading plays only a minimal role. The resultant fit as given by (3.1) was found to agree with the data points comprising the individual distributions at the four path elevation angles to within 1 dB.

In Table 3.1 is given a listing of M and N values for elevation angles ranging from 20° to 60° at 5° intervals which may be applied to (3.1). In Figure 3.3 are shown a family of cumulative distributions for the indicated path elevation angles.

In Figure 3.4 are plotted the fade exceeded versus the path elevation angle for a family of isopleths of constant percentages; namely, 1, 2, 5, 10, and 20%. These curves were derived from (3.1) and may be expressed by the alternate form of the ERS formulation given by

$$\mathrm{A}(\theta, \mathrm{P}) = \alpha(\mathrm{P}) + \beta(\mathrm{P})\theta + \gamma(\mathrm{P})\theta^2 \tag{3.5}$$

where A is the fade exceed (in dB), θ is the path elevation angle (in degrees), and where $\alpha(\mathrm{P})$, $\beta(\mathrm{P})$, and $\gamma(\mathrm{P})$ are tabulated in Table 3.2 for the indicated percentage levels, P. The above formulation was found to be in agreement with the original set of median distributions

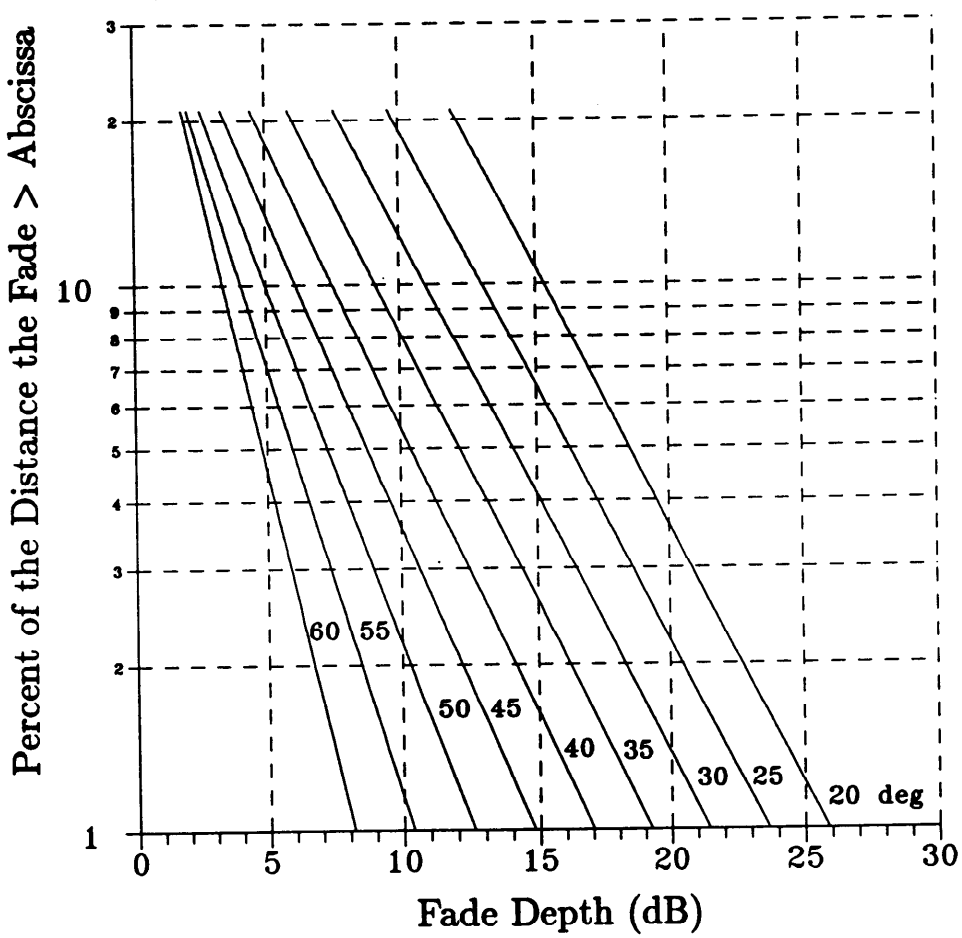

Figure 3.3: Cumulative fade distributions at 1.5 GHz for family of path elevation angles derived from the Empirical Roadside Shadowing model.

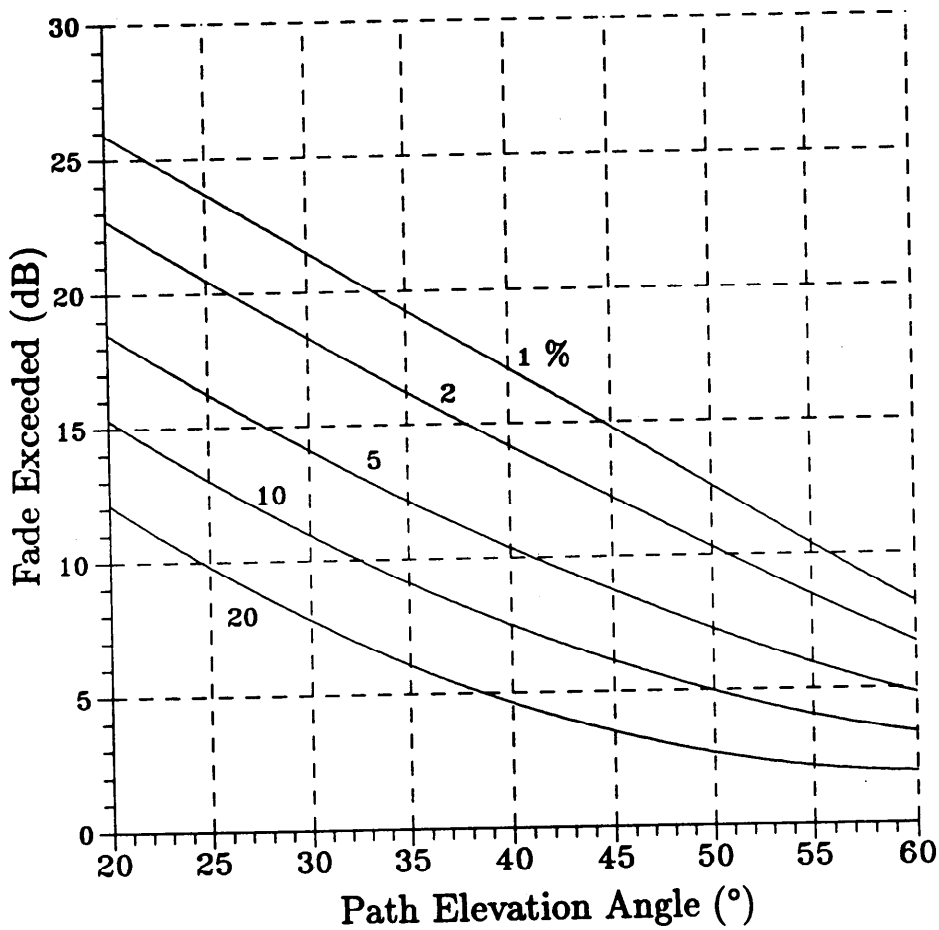

Figure 3.4: L-Band fade exceeded versus path elevation angle for family of indicated constant percentages (ERS model).

Table 3.2: Listing of parameter values α(P), β(P), and γ(P) in equation (3.5)

Percentage (P)	α(P)	β(P)	γ(P)
20	24.45	−0.7351	5.991×10^{-3}
10	26.84	−0.6775	4.605×10^{-3}
5	29.22	−0.6000	3.219×10^{-3}
2	32.38	−0.5106	1.386×10^{-3}
1	34.76	−0.4430	0

at 21°, 30°, 45°, and 60° to within 0.3 dB.

As previously mentioned, a description of fade statistics at smaller elevation angles becomes increasingly complex as it may involve absorption and scattering due to multiple canopies and tree trunks and approach the scenario depicted in Figure 2.2. Application of the ERS model at smaller elevation angles is therefore not suggested .

3.4 Validation of the Empirical Roadside Shadowing Model

It is interesting to compare the ERS model with distributions obtained from measurements made in Australia by the authors [Vogel et al., 1989]. Two major vegetation zones were traversed in Australia; forests along the coastal roads and woodlands further inland. Forests ranged from dry sclerophyll, in which the crowns of contiguous trees do not touch each other to tropical rain-forests, in which the leafy crowns of the trees intermingle. The dominating tree genus in the forest was Eucalyptus. Other than tree types, general similarities existed between the roads traveled in Australia and those in Central Maryland (e.g., tree heights, percentage of optical shadowing, setbacks).

In Table 3.3 are given the transmitter and receiver system parameters for the Australian campaign. In Figure 3.5 are plotted the fade distribution for 403 km of road measurements comprising 15 individual runs using ETS-V. The common characteristic of each run was that at 1% of the distance traveled, 10 dB was exceeded. Also plotted for comparison is the

Table 3.3: Summary of Pertinent Transmitter-Receiver System Parameters for Australian Campaign [Vogel et al., 1991].

Transmitter Platform #1	ETS-V
Azimuth at Sydney	−2°
Elevation at Sydney	51°
Frequency (MHz)	1545.15
EIRP (dBW)	25.9
Polarization	LHCP
Transmitter Platform #2	INMARSAT Pacific
Azimuth at Sydney	45°
Elevation at Sydney	40°
Frequency (MHz)	1541.5
EIRP (dBW)	20
Polarization	RHCP
Receiver Antennas (Low Gain)	Crossed Drooping Dipole
Gain (dB)	4
Elevation Beamwidth	15° to 75°
Azimuth Beamwidth	Omnidirectional
Polarizations:	
ETS-V	LHCP
INMARSAT Pacific	RHCP
Receiver Antennas (High Gain)	Helix
Gain (dB)	14
Beamwidths (Principal Planes)	45°
Polarizations:	
ETS-V	LHCP
INMARSAT Pacific	RHCP
Receiver Bandwidths:	
Quadrature Detectors (Hz)	1000
Filter (Hz)	200
Signal to Noise Ratios (dB):	
ETS-V (Low Gain)	22.4
ETS-V (High Gain)	32.4
INMARSAT Pacific (Low Gain)	16.5
Sampling Rate (KHz)	1
Data Recorded	Quadrature Detector Outputs 200 Hz Filter Output Vehicle Speed Time

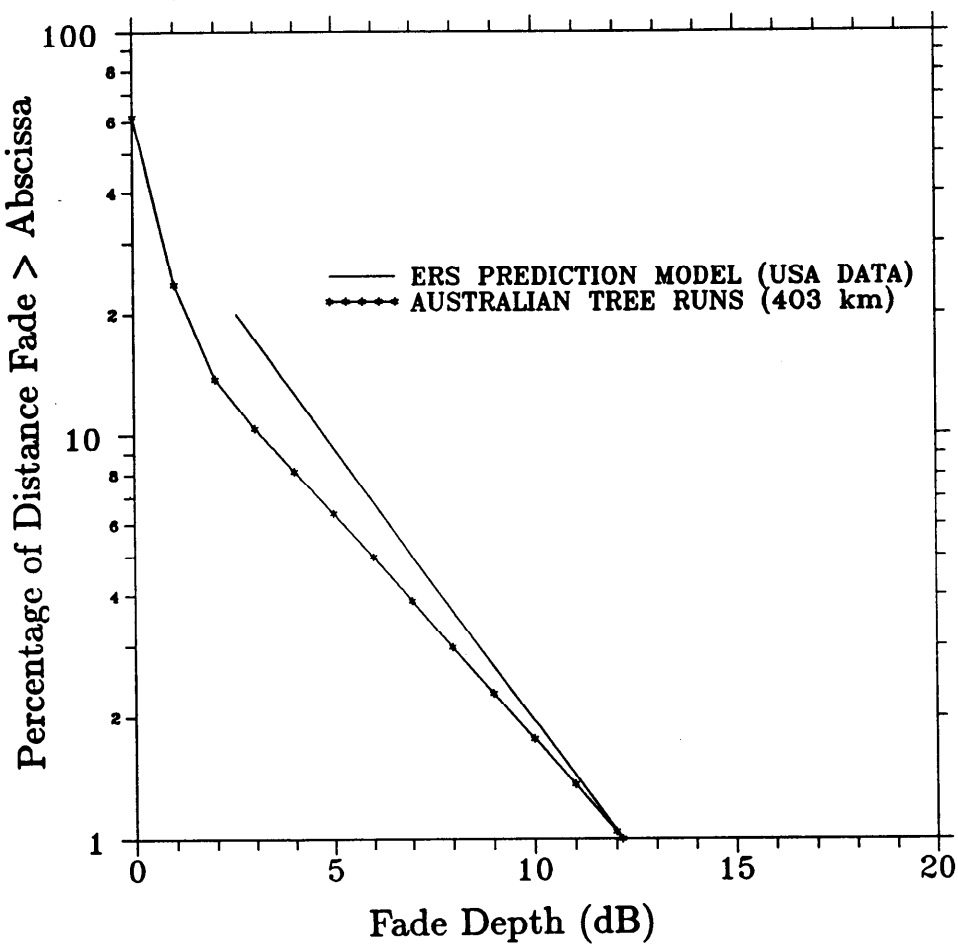

Figure 3.5: Comparison of Australian fade distribution comprising 15 runs with ERS model.

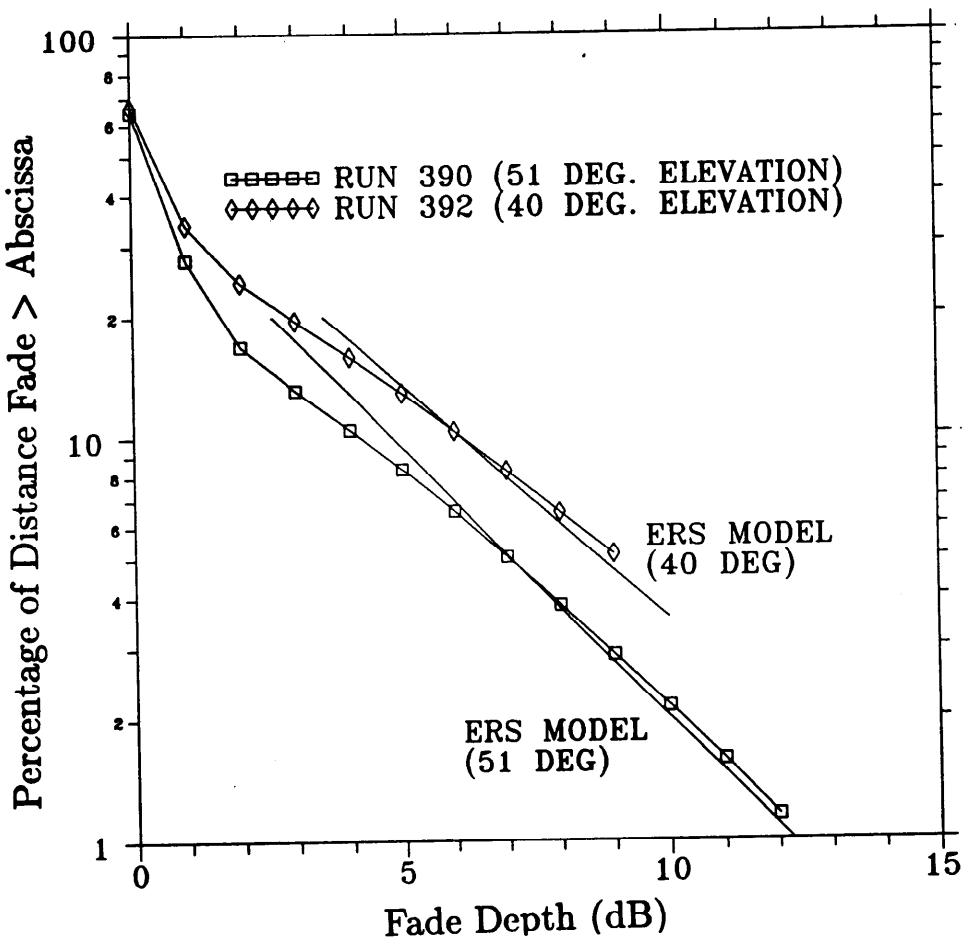

Figure 3.6: ERS and Australian fade distributions for different elevation angles from measurements obtained with INMARSAT Pacific (40°) and ETS-V (51°).

fade distribution as predicted by the ERS model (at 51°). We note the maximum difference between the two distributions is less than 2 dB at the 14% probability level, and thereafter this difference monotonically reduces.

In Figure 3.6 are distributions applied to separate runs along a tree lined road ($\approx$ 55 km) in which different satellites were accessed sequentially; INMARSAT-Pacific (elevation angle = 40°) and ETS-V (elevation angle = 51°). For both distributions, the fade differences (relative to the model) are less than 1 dB over the percentage range of validity.

3.5 L-Band Versus UHF Attenuation Scaling Factor: Dynamic Case

Simultaneous mobile fade measurements by the authors [Goldhirsh and Vogel, 1989; Vogel and Hong, 1988] at L-Band (1.5 GHz) and UHF (870 MHz) have demonstrated that the ratio of fades (fades are in dB) are approximately consistent with the ratio of the square root of frequencies. Hence,

For P = 1% to 30%

$$A(f_L) = A(f_{UHF})\sqrt{\frac{f_L}{f_{UHF}}} \qquad \text{(dB)} \tag{3.6}$$

For f_L = 1.5 GHz, f_{UHF} = 870 MHz

$$A(f_L) \approx 1.31 A(f_{UHF}) \qquad \text{(dB)} \tag{3.7}$$

The above result represents an overall average condition derived from 24 measurement runs along tree-lined roads in Central Maryland [Goldhirsh and Vogel, 1989]. The runs comprise path elevation angles of 30°, 45°, and 60° and a driving distance of 480 km. The multiplying coefficient 1.31 in (3.7) was shown to have an rms deviation of ± 0.1 over a fade exceedance range from 1% to 30%. As mentioned in Section 2.3, the result (3.6) for the dynamic case is consistent with (2.1) for the static case.

The multifrequency measurements of Bundrock and Harvey [1988] represent an independent validation of (3.6). In Table 3.4 are the 1% and 10% fade levels derived from simultane-

Table 3.4: Fades at the 1% and 10% levels derived from the multifrequency measurements of Bundrock and Harvey [1988]. Also shown in parentheses are the predicted levels employing frequency scaling and the UHF values.

Percentage	893 MHz	1550 MHz	2660 MHz
1	8.8	11.4 (11.6)	16.1 (15.2)
10	4.6	5.5 (6.1)	8.3 (7.9)

ous measurements made by them in Australia at 893 MHz, 1550 MHz, and 2660 MHz. Also shown in parentheses are the fade levels derived employing the UHF fades and expression (3.6). We note that overall agreement is quite good with an overall average percent error of less than 6% and a peak error smaller than 1 dB. Predictability even exists at the S-Band frequency, giving smaller than a 6% peak error.

3.6 Seasonal Effects on Attenuation – Dynamic Case

It may be recalled from Section 2.4, that a 35% increase in the attenuation was experienced at 870 MHz when comparing attenuation from trees having no foliage and those having foliage (winter versus summer). This case corresponded to a configuration in which the vehicle was stationary and the propagation path intersected the canopy. Seasonal measurements were also performed by the authors for the dynamic case in which the vehicle was traveling along a tree-lined highway in Central Maryland (Route 295) along which the propagation path was shadowed over approximately 75% of the road distance [Goldhirsh and Vogel, 1987; 1989]. Cumulative fade distributions were performed in March 1986 during which the deciduous trees were totally without foliage. These were compared with similar distributions acquired on October 1985 and June 1987, during which the trees were approximately in 80% and full blossom stages, respectively. The results may be expressed by

f = 870 MHz, P = 1% to 30%

$$A(\text{full foliage}) = 1.24A(\text{no foliage}) \qquad (\text{dB}) \tag{3.8}$$

Equation (3.8) states that over the exceedance range 1% to 30% of the seasonal cumulative distributions, there is an average increase in the dB fade of 24% ± 2% rms relative to fades from trees with no leaves.

The percentage fade increase (seasonal) for the dynamic case (24%) is less than that for the static case (35%) because the dynamic case has associated with it measurements which include evergreens (minimal seasonal change) and some stretches of road over which their were no trees. The static case also represents a maximum attenuation condition, whereas the dynamic case is expressed in terms of cumulative distributions. Although the above measurements have been made at 870 MHz, the result should not be significantly different at 1.5 GHz.

3.7 Fade Reduction Due to Lane Diversity

We examine the extent by which the fade reduces (or increases) by switching lanes for LMSS configurations. Figures 3.7 (a) and (b) show vehicles driving on the right and left lanes, respectively, where the satellite is to the right and the propagation path passes through the tree canopy on the right side of the road. We note that the path length through the canopy is greater when the vehicle is closest to the tree line (right side of road for examples given). A fade reduction should therefore be experienced by switching lanes from the right to the left side. The authors measured this effect at UHF (870 MHz) [Goldhirsh and Vogel, 1987], and L-Band (1.5 GHz) [Goldhirsh and Vogel, 1989]. Repeated distributions from helicopter measurements were derived for left and right lane driving at fixed path elevation angles of 30°, 45°, and 60°. A quantity defined as the "fade reduction, FR" is used to characterize the increase in signal power gained by switching lanes. This quantity is obtained by differencing equi-probability fade values from distributions pertaining to right and left side driving. The fade reductions at L-Band and UHF are plotted in Figures 3.8 and 3.9 as a function of the equal probability maximum fades. The maximum fades were derived from the distribution for the right lane driving case as shown in Figure 3.7 (a).

At each of the elevation angles, the individual data points have been replaced by the "best third order polynomial fit" which may be expressed by

<u>f = 1.5 GHz and 870 MHz</u>

$$FR = a_o + a_1 A + a_2 A^2 + a_3 A^3 \tag{3.9}$$

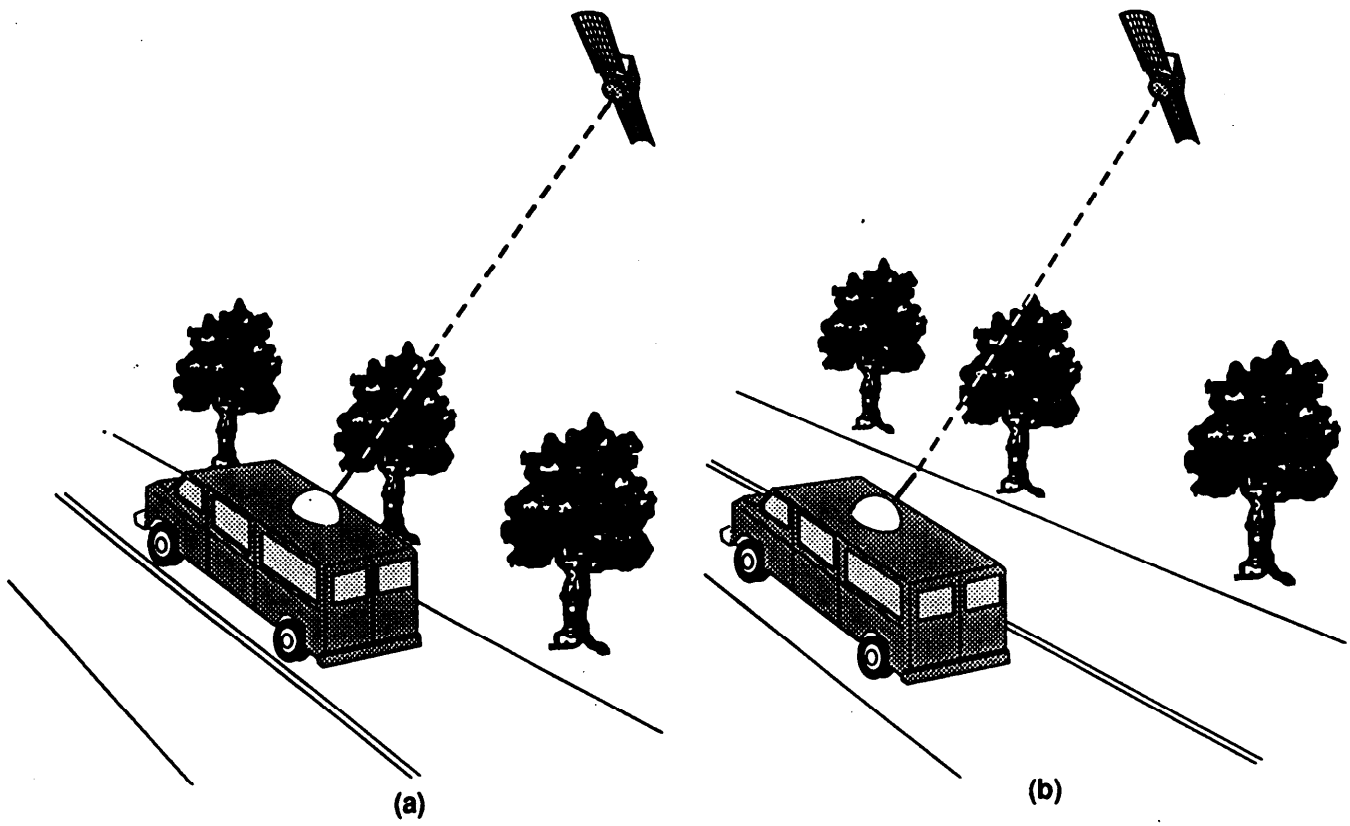

Figure 3.7: Mobile-satellite configurations depicting (a) larger intersecting path length with tree canopy when vehicle is driven in the right lane, and (b) smaller intersecting path length when vehicle is driven in the left lane.

where FR (in dB) represents the fade reduction obtained in switching lanes from the greater shadowing configuration (Figure 3.7 (a)) to the lesser one (Figure 3.7 (b)). Also, a_o, a_1, a_2, and a_3 are tabulated in Tables 3.5 and 3.6 for L-band and UHF, respectively. The parameter A (in dB) represents the maximum fade level value (derived for the configuration in Figure 3.7 (a)). The "best fit polynomials" were observed to agree with FR as derived from the measured distributions to within 0.1 dB rms.

It is interesting to note that larger fade reductions occur the greater the elevation angle. This arises because at the larger angles a change of lanes may radically alter the earth-satellite path from a shadowed to a non-shadowed condition (Figure 3.7). At the lower elevation angles, this change of conditions becomes less likely.

Table 3.5: Coefficients of fade reduction formulation (3.9) for lane diversity at f = 1.5 GHz.

El. Angle θ (deg)	a_o	a_1	a_2	a_3	dB Range
30	0.2818	0.2840	-1.876×10^{-2}	4.811×10^{-4}	3–25
45	−1.073	0.8816	-4.651×10^{-2}	7.942×10^{-4}	3–17
60	-4.206×10^{-2}	0.1671	6.602×10^{-2}	-2.720×10^{-3}	3–15

Table 3.6: Coefficients of fade reduction formulation (3.9) for lane diversity at f = 870 MHz.

El. Angle θ (deg)	a_o	a_1	a_2	a_3	dB Range
30	5.020×10^{-3}	.3354	-2.439×10^{-2}	7.764×10^{-4}	2–20
45	−0.8193	0.8430	-5.758×10^{-2}	1.222×10^{-3}	2–12
60	−0.2004	0.2112	7.076×10^{-2}	-3.764×10^{-3}	2–11

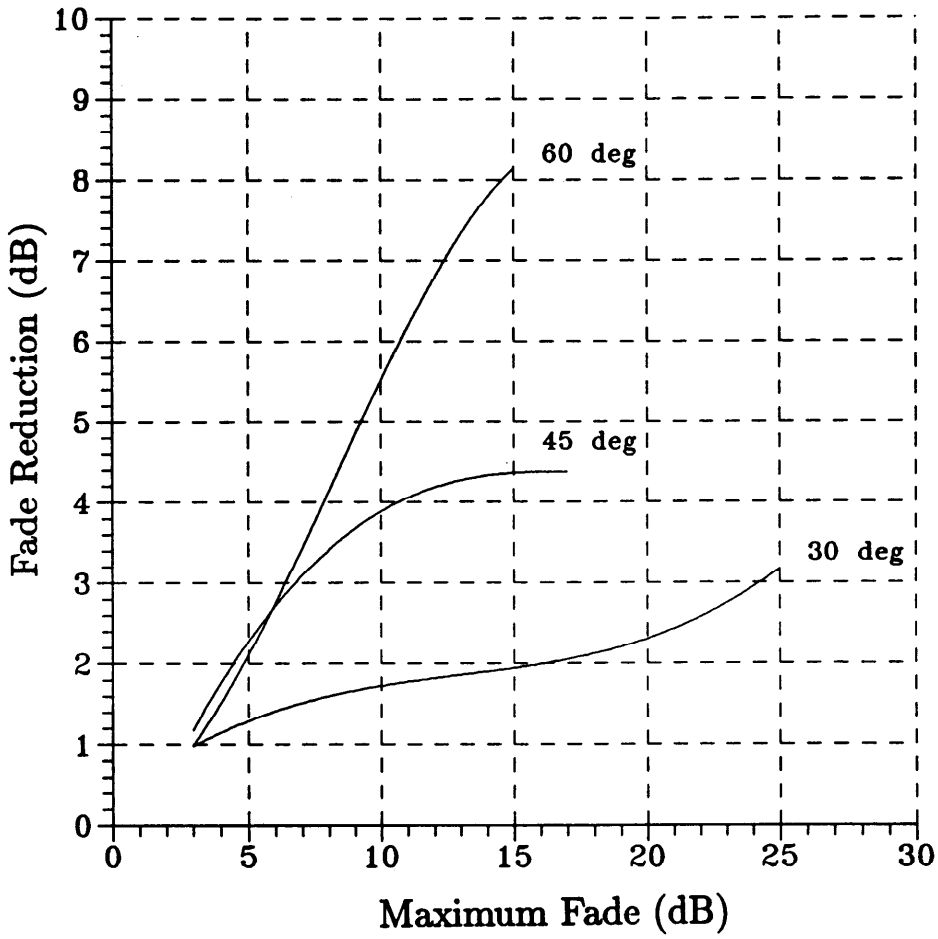

Figure 3.8: Best fit fade reduction at 1.5 GHz versus equi-probability attenuation at path elevation angles of 30°, 45°, and 60°.

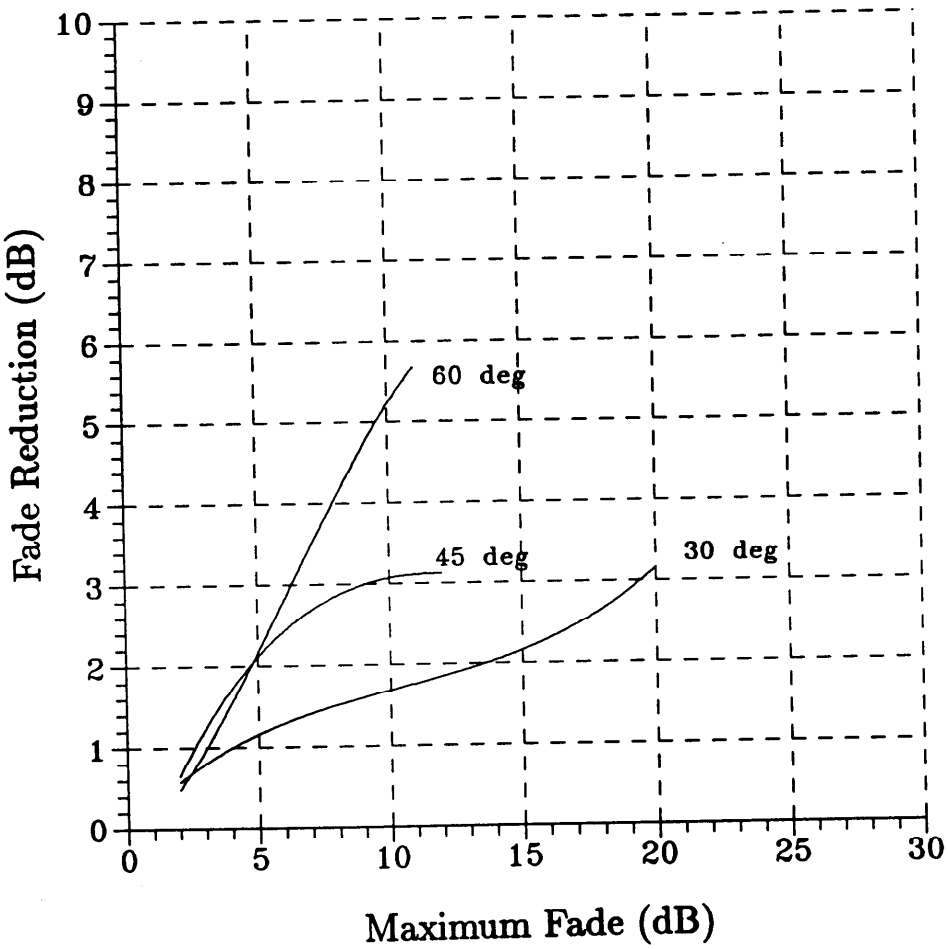

Figure 3.9: Best fit fade reduction at 870 MHz versus equi-probability attenuation at path elevation angles of 30°, 45°, and 60°.